Contemporary Mathematics
https://ojs.wiserpub.com/index.php/CM/

Research Article

Influence of Parameters on the Numerical Solution of Compressible Fluid Flow Around Obstacles Using a Meshless Method

Luminita Grecu

Department of Applied Mathematics, Faculty of Sciences, University of Craiova, Alexandru Ioan Cuza Street, No 13, 200585, Craiova, Romania
E-mail: lumigrecu@hotmail.com

Received: 27 May 2025; **Revised:** 14 July 2025; **Accepted:** 14 July 2025

Abstract: In this study numerical solutions for the compressible fluid flow around obstacles, based on a meshless method with Radial Basis Functions (RBFs) are presented. The numerical solutions are obtained by a hybrid method that uses the first step of the boundary element method, namely a singular boundary integral equation, which is an equivalent mathematical model for the problem of the compressible fluid around an obstacle, and then a meshless method based on RBFs for solving this singular boundary integral equation. Two types of RBFs are used, namely the Multiquadric RBFs and Gauss-type RBFs. An analytical check is made in order to study the numerical solutions' accuracy. Using computer simulations, we compare our results with an analytical solution available for a specific case. We examine how different parameters used to obtain the numerical solutions affect their accuracy, and we compare these numerical solutions to determine which RBF is most suitable for this scenario. We also note that the shape parameters of RBFs have a great influence on numerical solutions accuracy and, through simulations, optimal values are found. For evaluating the integrals of singular kernels which appear, the truncation method is applied. The influence of the parameter used to evaluate these integrals is also highlighted in the paper.

***Keywords*:** singular boundary integral equation, optimal values, shape parameter, radial basis functions, Cauchy Principal Value (CPV)

MSC: 76G25, 65D12, 65N38, 65R20

1. Introduction

Finding numerical solutions of great accuracy for the mathematical models associated to different real life boundary value problems is a very challenging problem and different techniques were developed to reach this goal. Finding efficient numerical computer codes, in order to obtain these numerical solutions, is another challenge in the way of solving these problems. In order to reach these goals, in this paper we solve the problem of the compressible fluid flow around obstacles by a new, hybrid method which combines the first step in applying the Boundary Element Method (BEM) with a meshless method developed by using different types of Radial Basis Functions (RBFs). The current approach benefits both from the advantages brought by the application of the BEM method in solving problems of compressible fluid flow, and from those of using meshless methods. The accuracy of numerical solutions obtained with meshless methods based on RBFs is

DOI: https://doi.org/10.37256/cm.6520257307

influenced a lot by the parameters the RBFs depend on. In this paper, through simulations, optimal values for these shape parameters are deduced, values which improve numerical solutions' accuracy.

Compressible fluid flows arise in many practical applications form aerospace and aeronautical engineering, automotive engineering, flows through compressors and turbines, in many environmental and meteorological applications, wind turbines, medical applications as respiratory airflow modeling in high frequency ventilations and many others, everywhere where the compressibility of the fluid, of the air for example, is extremely important.

Many authors have been studied compressible fluid flows around obstacles, and were focused on finding better and better numerical solutions for this problem. Different techniques have been applied to solve such problems: the Finite Element Method (FEM) [1], the Finite Difference Method (FDM) [2], BEM [3] and others. In many papers dealing with fluid flows, the velocity potential or the stream function are considered to be the unknowns of the problem. In [4], BEM is applied, in order to solve the problem of compressible flows around obstacles, a problem modelled through a system of partial differential equations with a nonlinear boundary condition, starting with the primary variables of the problem, namely the components of the perturbation velocity. There, the Singular Boundary Integral Equations Deduced (SBIEs) are numerically solved by a collocation method. In [5–7] different types of higher order boundary elements (as quadratic and cubic) are used to find numerical solutions for the mentioned SBIEs. In these approaches, by using isoparametric boundary elements, the unknown of the problem and also the boundary are approximated locally by models that follow a quadratic, respectively a cubic variation law which have local a quadratic, respectively a cubic approximation model.

When applying BEM, as described in many papers, as for example [3, 8], two important steps need to be done. The first step consists in finding an equivalent mathematical model for the problem to be solved, a model which represents a boundary integral formulation, usually a singular one, which incorporates the boundary conditions. During the second step the boundary is discretized and local approximations models for problem's unknown are introduced, so using different types of boundary elements numerical solutions for the integral equation are found.

In the herein work, a new numerical model is developed for the mentioned problem. Starting with the Singular Boundary Integral Equation (SBIE) with sources distribution, obtained in [4] by an indirect BEM, and solving it, with a meshless method which uses RBFs for the unknown approximation, its numerical solution is found.

From the family of RBFs, we choose two types of infinitely smooth RBFs: the Multiquadric RBFs (MQ RBFs, simply MQ) and the Gaussian RBFs (GA). Comparisons between different numerical solutions are made in order to find which type of RBFs offers better results. In [9] the GA were used to solve the same problem, but for the boundary discretization, boundary elements of linear type were utilised, so the boundary of the obstacle is there approximated by a closed polygonal line.

In approximation problems RBFs have proven to be effective tools. They are very often used for handling large scatter data [10], for finding solutions of PDEs [11, 12], and for integral equations [13], in computational fluid dynamics [14], and for compressible viscous flow in axisymmetric tubes [15], for approximating surfaces, in nonlinear approximations, in computational physics [16], in neural networks, the analysis of patterns and objects recognition and other applications on computers, and in many other approximations applications [17, 18], even in artificial intelligence applications, in machine learning algorithms. Together with, for example, eigenfunctions expansions, they are usually used in case of "meshless methods". These methods represent a family of approximations methods that approximate the unknowns by a set of basis functions, rather than discretizing the involved domain.

A function with real values, whose expression depends on two factors: the distance from the argument to a center, which is a fixed point, and a control parameter, named shape parameter, represents a radial basis function. This shape parameter can be modified in order to change the appearance and implicitly the behavior of the function. When using RBFs for solving an approximation problem, any function from the space of the unknown functions is represented as a linear combination of a set of linear independent RBFs, considered the base of that space. In this paper there are considered two infinitely smooth BRFs, namely the Gaussian RBFS (GA), and the Multiquadric RBFS (MQ).

We investigate in this paper, through simulations, how the shape parameters and the type of RBFs influence numerical solutions accuracy by considering the numerical solutions obtained through the present approach and comparing them with an exact one, known for a certain particular case. The shape parameter significantly affects the accuracy of the numerical

solution and so the problem of finding optimal values for this parameter is of great importance. The shape parameter has a major impact on the accuracy of the numerical solution.

Different methods for finding optimal values for shape parameters were proposed in many studies, but they were mainly used for functions interpolation, as for example trial and error, or Rippa's algorithm based on the idea of cross validation [19]. Some formulas for finding such optimal values were also proposed by certain authors, as for example Hardy [20] and others.

Finding optimal values for the shape parameter in case of solving partial differential equations or integral ones by using RBFs is an even more challenging task. Many papers study the influence of these parameters and most optimal values for the shape parameters are found by numerical experiments. In [21] an extension of Rippa's Leave-One-Out Cross Validation (LOOCV) algorithm is applied for partial differential equations. Another extension of the cross validation algorithm is proposed in [22]. In [23] different methods that should lead to a better conditioning of the systems to be solved are discussed, as for example a method that uses variable MQ shape parameters related to the local radius of curvature, which improves the accuracy of the numerical solution. In [24] some intervals for optimal shape parameter values are experimentally highlighted in the case of using MQ RBFs for solving linear integral equations. In [25] a Sample Solution Approach (SSA) is proposed for achieving a reasonably good shape parameter in case of MQ-RBF. The procedure is based on finding a pseudo-problem whose solution is known, obtaining the optimal parameter of the MQ-RBF for the pseudo-problem and considering that the optimal shape parameter of the pseudo-problem can also achieve an approximately optimal accuracy in the solution of the original problem.

In paper [26] the authors use GA and Inverse Multiquadric functions (IMQ) in their approach and show, for some concrete situations, that if the shape parameter is equal with 2, in the case of using GA, the numerical results are very good, without presenting details related to how this value is chosen.

In [27] the authors use neural networks to determining methods for obtaining optimal values of the control parameter, for the case of RBFs interpolation problems, and, based on an unsupervised learning strategy, they get these values for two RBFs: the inverse multiquadric and the Gaussian.

Other strategy to obtain optimal values for the shape parameter is proposed in paper [28] and is based on transforming the initial problem to a one-dimensional minimization problem, for which the variable to be optimized is the control parameter. Here, for the considered numerical cases the optimal values of the shape parameter are $c = 0.26$; (d) $c = 0.28$, optimal value for Gaussians, but very good results are obtained when this parameter was situated in the studied range, namely [0, 1; 1].

Because finding optimal values for the shape parameter is a difficult problem, many of the authors who use RBFs in their approaches avoid using classical functions (MQ, GA, IMQ and others) and turn to other RBFs such as the Polyharmonic Splines (PS RBFs), as in papers [29, 30], to conical RBFs as in [31], or to other types of RBFs as in [32].

In the herein study we find, based on simulations and analytical checking, optimal values for the shape parameters in case of MQ RBFs and GA, taking advantage of the fact that an analytical solution to the studied problem is known, in a particular case.

After applying the first step of the BEM the equivalent integral model of the problem is a SBIE. Difficulties arise when evaluating singular integrals, but different methods can be used to overcome this difficulty, see for example [33].

Considering the fact that the SBIE is obtained based on the Cauchy Principal Value (CPV) concept, the integrals with singular kernels are evaluated using the truncation method. When applying the truncation method, a small parameter, eps, is used to isolate and to eliminate the singularity. The analysis of how this parameter influences the accuracy of the numerical solutions is also presented in the paper.

2. Methods

In this section the proposed hybrid procedure for obtaining the numerical solution for the problem of the compressible fluid flow around obstacles is presented. It is a procedure which combines the first step in applying the BEM and a meshless method with radial basis function to solve the resulting SBIE.

2.1 *The SBIE with sources distributions*

A brief presentation of both the problem to be solved and the integral equation resulting from the application of the first step of BEM is presented below, but a more detailed presentation can be found in [4].

We want to find a numerical solution for the perturbation velocity induced by the presence of a fixed body of a known boundary, assumed to be smooth and closed, noted C in a compressible fluid, that has, at great distances from the body, a uniform, steady, potential motion of subsonic velocity. After finding the perturbation velocity field the fluid action on the body is obtained.

Replacing the obstacle boundary with a continuous distribution of sources of intensity f, which satisfies a Hölder condition on C, the problem is equivalent with the following SBIE, obtained in [4]:

$$\left(n_x^{0^2}+\beta^2 n_y^{0^2}\right) f(\bar{x}_0)+\frac{1}{\pi} CPV \oint_C f(\bar{x}) \frac{(x-x_0) n_x^0+\beta^2 (y-y_0) n_y^0}{\|\bar{x}-\bar{x}_0\|^2} ds = 2\beta n_x^0 \tag{1}$$

This SBIE is obtained in [4] following these three steps:

• First, the expressions of u, v, the perturbation velocity along the axes are found, in point $Q(\bar{x})$, from the domain of the fluid;

• Then, for a regular point on the boundary, $Q_0(\bar{x}_0) \in C$ (briefly named $\bar{x}_0 \in C$), u and v are deduced by the limits of the previous expressions, calculated as x_0 approaches to C;

• Finally, these expressions are forced to satisfy the nonlinear boundary condition on C.

CPV in (1) denotes the Cauchy Principal Value of an integral, and its definition can be found, for example, in [4], being in accordance with its classical definition which can be found in many works.

$$CPV \oint_C = \lim_{r \to 0} \oint_{C-c} \tag{2}$$

where $c = C \cap D(Q_0,\ r)$ and $D(Q_0,\ r)$ is a disc centered in $Q_0(\bar{x}_0)$, of radius r, which isolates the regular point, $n_x^0,\ n_y^0$ are the components of the normal unit vector, outward the fluid at $\bar{x}_0 \in C,\ \beta = \sqrt{1-M^2}$, and $M \in [0,\ 1)$ Mach number for the unperturbed fluid flow, and obviously f, the unknown function of the problem, represents the sources' intensity.

For solving the SBIE (1) a meshless method based on different RBFs, namely MQ and GA is developed in this work.

Denoting by $\tau(\bar{x}_0) = \left(n_x^0\right)^2 + \beta^2 \left(n_y^0\right)^2$ and by $K(\bar{x},\ \bar{x}_0) = \frac{1}{\pi} \frac{(x-x_0) n_x^0+\beta^2 (y-y_0) n_y^0}{\|\bar{x}-\bar{x}_0\|^2}$, equation (1) becomes:

$$\tau(\bar{x}_0) f(\bar{x}_0) + \text{CPV} \oint_C f(\bar{x}) K(\bar{x},\ \bar{x}_0)\, ds = 2\beta n_x^0 \tag{3}$$

2.2 *Solving the SIBE by reducing it to a linear system of equations*

First, we choose N nodes on the boundary, $\bar{x}_i,\ i = \overline{1,\ N},\ \bar{x}_{N+1} = \bar{x}_1$, and we require that the equation is satisfied in these nodes. So equation (3) becomes:

$$\tau(\bar{x}_i) f(\bar{x}_i) + \text{CPV} \oint_C f(\bar{x}) K(\bar{x},\ \bar{x}_i)\, ds = 2\beta n_x^i,\ i = \overline{1,\ N} \tag{4}$$

n_x^i being the component of the normal vector at $\bar{x}_i \in C$, along Ox.

We introduce in (4) the global model of approximation for the unknown function f, based on RBFs, so we consider an approximation of the following form:

$$f(\bar{x}) = \sum_{j=1}^{N} \lambda_j \varphi_j(\bar{x}), \tag{5}$$

where $\varphi_j(\bar{x})$ are the RBFs and λ_j are the weights. As the expressions of RBFs are known, weights become the coefficients to be found.

Introducing relation (5) in equation (4) we get the following form of it:

$$\tau(\bar{x}_i) \sum_{j=1}^{M} \lambda_j \varphi_j(\bar{x}_i) + \sum_{j=1}^{M} \text{CPV} \oint_C \lambda_j \varphi_j(\bar{x}) K(\bar{x}, \bar{x}_i)\, ds = 2\beta n_x^i,\ i = \overline{1, N} \tag{6}$$

The following linear system of N equations and N unknowns, the weights of the RBFs, is obtained:

$$\tau(\bar{x}_i) \sum_{j=1}^{N} \lambda_j \varphi_j(\bar{x}_i) + \sum_{j=1}^{N} \text{CPV} \oint_C \lambda_j \varphi_j(\bar{x}) K(\bar{x}, \bar{x}_i)\, ds = 2\beta n_x^i,\ i = \overline{1, N} \tag{7}$$

We then consider a parametrization for C: $x = x(\rho)$, $y = y(\rho)$, $\rho \in I$, and we have: $\bar{x}_i(x_i, y_i) = \bar{x}_i(\rho_i),\ x_i = x(\rho_i)$, $y_i = y(\rho_i)$, $\rho_i \in I,\ i = \overline{1, N}$ being parameter values corresponding to the nodes chosen on the boundary.

If we do not have a parametric representation but we know the position of some points on the boundary, C, we can approximate the boundary by a closed polygonal line, as in paper [9], and we can then proceed to find a numerical solution of the SBIE.

Denoting by

$$H_j(\bar{x}(\rho), \bar{x}(\rho_i)) = \varphi_j(\bar{x}(\rho)) K(\bar{x}(\rho), \bar{x}(\rho_i))\ \sqrt{x'(\rho)^2 + y'(\rho)^2} \tag{8}$$

we get the following expression for equations (7):

$$\sum_{j=1}^{N} \lambda_j\ \tau(\bar{x}(\rho_i))\, \varphi_j(\bar{x}(\rho_i)) + \sum_{j=1}^{N} \lambda_j \text{CPV} \oint_C H_j(\bar{x}(\rho), \bar{x}(\rho_i))\, d\rho = 2\beta n_x^i \tag{9}$$

The accuracy of numerical results depends on the way of evaluating integrals with singularities. Singularities' evaluation can be made through different techniques: with special purpose quadrature formulas, orthogonal polynomials, subtracting the singularity, through analytical transformations, modified shape functions, truncated Taylor series, changes of coordinates, and other regularization techniques like methods of moments.

In this paper we evaluate the singular integrals that appear by using truncation method. As specified in [34] this method offers very good results in case when the integrand doesn't oscillate near the singularities, as it is the one in our case.

So, we evaluate the integrals with singular kernels by subtracting the singularity, as in the CVP definition, for each $i = \overline{1, N}$, using a small parameter, noted eps, to isolate the singularity. By definition:

$$CPV \oint_C H_j(\bar{x}(\rho), \bar{x}(\rho_i))\, d\rho = \lim_{eps \to 0} \left(\int_a^{\rho_i - eps} H_j(\bar{x}(\rho), \bar{x}(\rho_i))\, d\rho + \int_{\rho_i + eps}^{b} H_j(\bar{x}(\rho), \bar{x}(\rho_i))\, d\rho \right), \tag{10}$$

where $I = [a,\ b]$ is the corresponding boundary parameter's range.

Equations (9) become:

$$\sum_{j=1}^{N} \lambda_j\ \tau\left(\bar{x}(\rho_i)\right) \varphi_j\left(\bar{x}(\rho_i)\right) + \sum_{j=1}^{N} \lambda_j \lim_{eps \to 0} \left(\int_a^{\rho_i - eps} H_j\left(\bar{x}(\rho),\ \bar{x}(\rho_i)\right) d\rho + \int_{\rho_i + eps}^{b} H_j\left(\bar{x}(\rho),\ \bar{x}(\rho_i)\right) d\rho \right) = 2\beta n_x^i \quad (11)$$

For the numerical computing of the above integrals we use the following rule:

$$CPV \oint_C H_j\left(\bar{x}(\rho),\ \bar{x}(\rho_i)\right) d\rho = \int_a^{\rho_i - eps} H_j\left(\bar{x}(\rho),\ \bar{x}(\rho_i)\right) d\rho + \int_{\rho_i + eps}^{b} H_j\left(\bar{x}(\rho),\ \bar{x}(\rho_i)\right) d\rho, \quad (12)$$

Denoting by:

$$q_{ij} = \tau\left(\bar{x}(\rho_i)\right) \varphi_j\left(\bar{x}(\rho_i)\right),\ c_{ij} = \int_a^{\rho_i - eps} H_j\left(\bar{x}(\rho),\ \bar{x}\left(\rho^i\right)\right) d\rho + \int_{\rho_i + eps}^{b} H_j\left(\bar{x}(\rho),\ \bar{x}\left(\rho^i\right)\right) d\rho, \quad (13)$$

$$a_{ij} = q_{ij} + c_{ij},\ i,\ j \in \{1,\ \ldots,\ N\},\ A = (a_{ij})_{1 \le i,\ j \le N},\ \{\lambda\} = (\lambda_1\ \lambda_2 \ldots \lambda_N)^T, \quad (14)$$

$$B = \left(2\beta n_x^1\ 2\beta n_x^2 \ldots 2\beta n_x^N\right)^T \quad (15)$$

where $()^T$ represents the transpose of the corresponding line vector, namely a column vector from R^N, the problem is reduced to the following system of equations, written in (16) in a matricial form, whose unknowns are the weights $\lambda_j,\ j = \overline{1,\ N}$:

$$A \cdot \{\lambda\} = B \quad (16)$$

The evaluation of the coefficients of system (16), as well as its solution can be obtained with a computer code, one for each type of RBFs used for the unknown global approximation.

2.3 *Types of RBFs and systems coefficients evaluations*

RBFs depend only on the distances from current points to their centers, noted $\bar{c}$, and on a parameter, called shape parameter, which change the aspect of the functions: $\varphi\left(\bar{x}\right) = \varphi(r,\ \alpha) = \varphi\left(\|\bar{x} - \bar{c}\|,\ \alpha\right)$.

In the present study there are used two type of RBFs: MQ RBFs and the GA RBFs. They have the following expressions:

- $\varphi_j\left(\bar{x}\right) = \sqrt{\left\|\bar{x} - \bar{c}_j\right\|^2 + \alpha^2}$, in case of MQ RBFs,
- $\varphi_j\left(\bar{x}\right) = e^{-\alpha^2 \left\|\bar{x} - \bar{c}_j\right\|^2}$, in case of GA RBFs,

$\bar{c}_j$ representing, in both situations, the center of φ_j.

In this approach we consider the centers to be the nodes chosen on the boundary, so we consider that $\varphi_j\left(\bar{x}\right)$ has the center in $\bar{x}_j,\ \overline{c_j} = \bar{x}(\rho_j),\ j = \overline{1,\ N}$. Introducing the above expressions of RBFs in equations (15) all systems' coefficients can be evaluated with a computer code.

The coefficients obtained, for each of these two situations, are presented in (18), (20).

For MQ RBFs we get:

$$q_{ji} = \tau(\bar{x}(\rho_i)) \sqrt{\alpha^2 + \left\|\bar{x}(\rho) - \bar{x}(\rho_j)\right\|^2} \tag{17}$$

$$c_{ij} = \int_a^{\rho_i - \text{eps}} \sqrt{\alpha^2 + \left\|\bar{x}(\rho) - \bar{x}(\rho_j)\right\|^2} K(\bar{x}(\rho),\, \bar{x}(\rho_i)) J(\rho) d\rho$$

$$+ \int_{\rho_i + eps}^{b} \sqrt{\alpha^2 + \left\|\bar{x}(\rho) - \bar{x}(\rho_j)\right\|^2} K(\bar{x}(\rho),\, \bar{x}(\rho_i)) J(\rho), \tag{18}$$

For GA RBFs we obtain:

$$q_{ji} = \tau(\bar{x}(\rho_i)) e^{-\alpha^2 \left\|\bar{x}(\rho_i) - \bar{x}(\rho_j)\right\|^2} \tag{19}$$

$$c_{ij} = \int_a^{\rho_i - eps} e^{-\alpha^2 \left\|\bar{x}(\rho) - \bar{x}(\rho_j)\right\|^2} K(\bar{x}(\rho),\, \bar{x}(\rho_i)) J(\rho) d\rho$$

$$+ \int_{\rho_i + eps}^{b} e^{-\alpha^2 \left\|\bar{x}(\rho) - \bar{x}(\rho_j)\right\|^2} K(\bar{x}(\rho),\, \bar{x}(\rho_i)) J(\rho) d\rho \tag{20}$$

The above coefficients of system (16), as well as its solution, can be obtained with a computer code, but separately, for each type of RBFs used for the unknown global approximation. The computer code is similar for these two situations, differences appear only in coefficients expressions and can be easily adapted for other kinds of RBFs.

The system the problem is reduced at, must be solved with an iterative procedure in order to avoid an ill posed problem. In this paper the method which uses the concept of the general inverse of a matrix is used and, as will be seen, it offers good numerical results.

After solving this system, the perturbation velocity components can be evaluated.

3. The velocity field on the boundary

On the boundary the expressions for u and v are:

$$u(\bar{x}_0) = -\frac{1}{2} f(\bar{x}_0) n_x^0 - \frac{1}{2\pi} \text{CPV} \oint_C f(\bar{x}) \frac{x - x_0}{\left\|\bar{x} - \bar{x}_0\right\|^2} ds \tag{21}$$

$$v(\bar{x}_0) = -\frac{1}{2} f(\bar{x}_0) n_y^0 - \frac{1}{2\pi} \text{CPV} \oint_C f(\bar{x}) \frac{y - y_0}{\left\|\bar{x} - \bar{x}_0\right\|^2} ds, \tag{22}$$

After solving the system and finding the weights of the RBFs, we can evaluate the perturbation velocity components with the above relations (22), on the boundary, in the same manner as in case of obtaining the linear system of equations, introducing the approximation based on RBFS and considering $\bar{x}_0 = \bar{x}_i,\ i = \overline{1,\, N}$. Using the RBFs, they can be evaluated, on the N nodes chosen on the boundary, by relations:

$$u(\bar{x}_i) = -\frac{1}{2}\sum_{j=1}^{N}\lambda_j\varphi_j(\bar{x}_i)n_x^i - \frac{1}{2\pi}\sum_{j=1}^{N}\lambda_j \text{CPV}\oint_C \varphi_j(\bar{x})\frac{x-x_i}{\|\bar{x}-\bar{x}_i\|^2}ds \tag{23}$$

$$v(\bar{x}_i) = -\frac{1}{2}\sum_{j=1}^{N}\lambda_j\varphi_j(\bar{x}_i)n_y^i - \frac{1}{2\pi}\sum_{j=1}^{N}\lambda_j \text{CPV}\oint_C \varphi_j(\bar{x})\frac{y-y_i}{\|\bar{x}-\bar{x}_i\|^2}ds, \tag{24}$$

Using the same technique as in case of obtaining the previous system, we introduce in the above relations the parametric equations of boundary C: $x = x(\rho)$, $y = y(\rho)$, $\rho \in I$, $\rho_1, \ldots. \rho_N$, being the parameter's values for the N nodes, $\bar{x}_i(x_i, y_i) = \bar{x}_i(\rho_i)$, $x_i = x(\rho_i)$, $y_i = y(\rho_i)$.

Denoting by:

$$ds = \sqrt{x'(\rho)^2 + y'(\rho)^2}\,d\rho = J(\rho)d\rho \tag{25}$$

$$g^i(\rho) = \frac{x(\rho)-x(\rho_i)}{\|\bar{x}(\rho)-\bar{x}(\rho_i)\|^2},\ h^i(\rho) = \frac{y(\rho)-y(\rho_i)}{\|\bar{x}(\rho)-\bar{x}(\rho_i)\|^2}, \tag{26}$$

$$w_{ij} = \varphi_j(\bar{x}(\rho_i))n_x^i + \frac{1}{\pi}\text{CPV}\oint_C \varphi_j(\bar{x}(\rho))g^i(\rho)J(\rho)d\rho, \tag{27}$$

$$z_{ij} = \varphi_j(\bar{x}(\rho_i))n_y^i + \frac{1}{\pi}\text{CPV}\oint_C \varphi_j(\bar{x}(\rho))h^i(\rho)J(\rho)d\rho, \tag{28}$$

we get the expressions of the components of the perturbation velocity at the N nodes on the boundary:

$$u(\bar{x}_i) = -\frac{1}{2}\sum_{j=1}^{N}w_{ij}\lambda_j,\ i=\overline{1,\ N},\ v(\bar{x}_i) = -\frac{1}{2}\sum_{j=1}^{N}z_{ij}\lambda_j,\ i=\overline{1,\ N} \tag{29}$$

We further deduce the expressions of the perturbation velocity components for the two types of RBFs we use to solve the problem.

In case of MQ we have:

$$w_{ij} = \sqrt{\alpha^2 + \left\|\bar{x}(\rho_i)-\bar{x}(\rho_j)\right\|^2}n_x^i + \frac{1}{\pi}\text{CPV}\oint_C \sqrt{\alpha^2 + \left\|\bar{x}(\rho)-\bar{x}(\rho_j)\right\|^2}g^i(\rho)J(\rho)d\rho \tag{30}$$

$$z_{ij} = \sqrt{\alpha^2 + \left\|\bar{x}(\rho_i)-\bar{x}(\rho_j)\right\|^2}n_y^i + \frac{1}{\pi}\text{CPV}\oint_C \sqrt{\alpha^2 + \left\|\bar{x}(\rho)-\bar{x}(\rho_j)\right\|^2}h^i(\rho)J(\rho)d\rho \tag{31}$$

In case of GA, the coefficients used for obtaining the velocity components are:

$$w_{ij} = e^{-\alpha^2\left\|\bar{x}(\rho_i)-\bar{x}(\rho_j)\right\|^2}n_x^i + \frac{1}{\pi}\text{CPV}\oint_C e^{-\alpha^2\left\|\bar{x}(\rho)-\bar{x}(\rho_j)\right\|^2}g^i(\rho)J(\rho)d\rho \tag{32}$$

$$z_{ij} = e^{-\alpha^2 \left\| \bar{x}(\rho_i) - \bar{x}(\rho_j) \right\|^2} n_y^i + \frac{1}{\pi} \text{CPV} \oint_C e^{-\alpha^2 \left\| \bar{x}(\rho) - \bar{x}(\rho_j) \right\|^2} h^i(\rho) J(\rho) d\rho \tag{33}$$

For evaluating the Cauchy Principal Values of the involved singular integrals, the truncation method is used as in case of the system's coefficients. According to the CPV definition we have:

$$\text{CPV} \oint_C \varphi_j(\bar{x}(\rho)) F^i(\rho) d\rho = \lim_{eps \to 0} \left(\int_a^{\rho_i - eps} \varphi_j(\bar{x}(\rho)) F^i(\rho) d\rho + \int_{\rho_i + eps}^b \varphi_j(\bar{x}(\rho)) F^i(\rho) d\rho \right), \tag{34}$$

$F^i(\rho)$ having different expressions: $F^i(\rho) = g^i(\rho) J(\rho)$ in case of u, $F^i(\rho) = h^i(\rho) J(\rho)$ in case of v, φ_j being either a MQ or GA.

So, using truncation method, we choose a very small parameter, eps, and we numerically compute the CPV by the following rule:

$$\text{CPV} \oint_C \varphi_j(\bar{x}(\rho)) F^i(\rho) d\rho = \int_a^{\rho_i - eps} \varphi_j(\bar{x}(\rho)) F^i(\rho) d\rho + \int_{\rho_i + eps}^b \varphi_j(\bar{x}(\rho)) F^i(\rho) d\rho, \tag{35}$$

After finding the components of the perturbation velocity field we can compute the local pressure coefficient at any point on the boundary, as for example at $\bar{x}_i$, using the following relation, see [4]:

$$cp(\bar{x}_i) = \frac{2}{\gamma M^2} \left\{ \left[1 + \frac{M^2(\gamma - 1)}{2} \left(1 - v^2(\bar{x}_i) - \left(1 + \frac{u(\bar{x}_i)}{\beta} \right)^2 \right) \right]^{\frac{\gamma}{\gamma - 1}} - 1 \right\}, \; M \neq 0, \tag{36}$$

4. Numerical results

The proposed meshless methods for solving the SBIE with sources distribution, based on RBFs is implemented into computer codes using Mathcad programming language and, based on them, numerical solutions are obtained. For both cases the input data are: the number of nodes, N; the parametrization of the boundary C; eps the parameter used for singular integrals evaluation; shape parameter's value, α; Mach number, M, $(0 \leq M < 1)$.

Output data are: nodal values for the RBFs weights, the velocity field components and the local pressure coefficient.

As we have mentioned before a direct method to solve the linear system of equations cannot be applied, so we chose an iterative method to solve it. The iterative method based on the general (pseudo) inverse, which gives the least-squares solution to a system of equations, is implemented into a built-in function in Mathcad, namely *geninv* (*matrix*). Using this procedure, we overcome the problems which arise when the ill posed problems arise.

Results validation is done through an analytical checking, by considering a problem with an exact solution, and making comparisons between the numerical and the exact solutions. For the particular case of a circular obstacle, of radius one, centered in the origin, and an incompressible fluid flow ($M = 0$), the exact solution is given in [4]: $u = -\cos 2\theta$, $v = -\sin 2\theta$, $cp = -1 + 2\cos 2\theta$.

So, for testing the proposed method, we have considered a circular obstacle centered in the origin with radius one, as the smoothed boundary of the obstacle.

For every point, Q, on the boundary we have: $Q(cos\rho,\ sin\rho)$, $\rho \in [0,\ 2\pi]$. A uniform distribution for the control points is considered and we have as nodes on the boundary the points corresponding to $\rho_i = \dfrac{2i-1}{N}\pi$, so we evaluate

the velocity field and the local pressure coefficient at $Q_i\left(\cos\frac{2i-1}{N}\pi,\ \sin\frac{2i-1}{N}\pi\right)$ for both numerical and analytical solutions.

The two computer codes are developed in case of a circular obstacle: the first one for the case of MQ RBFS, and the second for the case of GA. The output data in this situation also include the errors between the numerical and the exact solution.

The error measure used to quantify the performance of the exposed method and to study the influence of parameters on the numerical solutions accuracy is considered to be the maximum absolute error, ($\|\bar{x}\|_\infty$). So we define:

$$Mu = \|\overline{eru}\|_\infty = \max_{i=1,\,N}\{eru(i)\},\ Mv = \|\overline{erv}\|_\infty = \max_{i=1,\,N}\{erv(i)\}, \tag{37}$$

$$Mcp = \left\|\overline{Ercp}\right\|_\infty = \max_{i=1,\,N}\{Ercp(i)\} \tag{38}$$

In (38), $eru(i)$, $erv(i)$, $Ercp(i)$ are the absolute errors between the numerical and the real values of the velocity components, respectively of the local pressure coefficient, evaluated at the i^{th} nodal point, and $\overline{eru}$, $\overline{erv}$, $\overline{Ercp}$ are the vectors of the mentioned absolute errors, evaluated in every nodal point.

4.1 *Numerical results in case of MQ RBFs*

Numerical results are compared with the exact ones in the following diagrams. First, we consider the numerical solution obtained in the case of MQ RBFs, and compare this solution with the exact one, in case of using only 20 nodes on the boundary, $eps = 0.01$ and $\alpha = 1$.

As we can see in Figure 1 a good agreement exists between the numerical solutions, marked with lowercase letters (u, v for the Ox, respectively Oy velocity components, cp for local pressure coefficient) and the exact ones, noted with capital letters (U, V and Cp respectively).

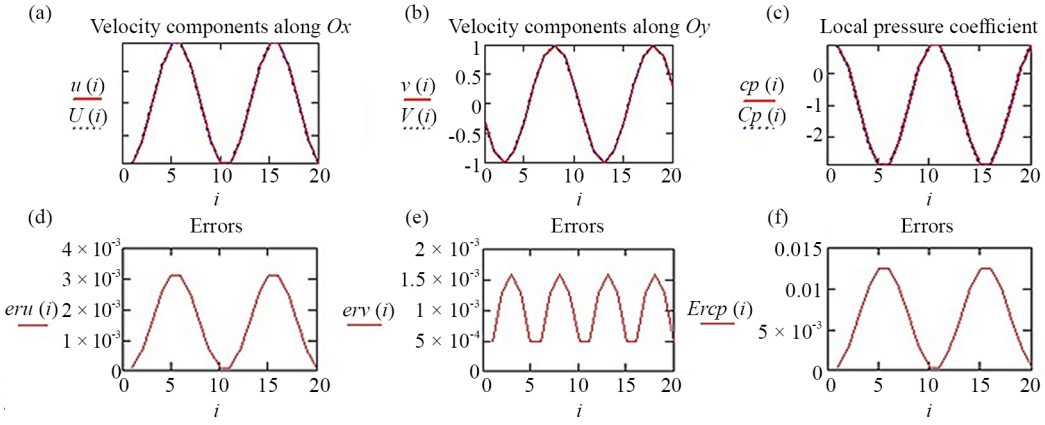

Figure 1. Numerical solution vs. exact one and the corresponding absolute errors, for MQ RBFs: $N = 20$ nodes, $eps = 0.01$, $\alpha = 1$

In Figure 1 the distribution of the absolute errors, $eru(i)$, $erv(i)$, $Ercp(i)$, for all three measures of interest, can also be observed.

4.1.1 *The influence of eps on numerical solution's accuracy (MQ case)*

The influence of eps on numerical solution's accuracy is highlighted in Table 1, where the results obtained for Mu, Mv, Mcp, in case of using 20 nodes on the boundary and $\alpha = 1$, for different values of eps parameter are presented.

Table 1. Max of the absolute errors ($\|\overline{eru}\|_\infty$, $\|\overline{erv}\|_\infty$ $\|\overline{Ercp}\|_\infty$) for different values of eps parameter: Mu, Mv, Mcp

No.	eps	Mu	Mv	Mcp
1	0.000001	3.11454E-07	1.6065E-07	1.24581E-06
2	0.00001	3.10615E-06	1.59305E-06	1.24246E-05
3	0.0001	3.1054E-05	1.59175E-05	0.000124215
4	0.001	0.00031062	0.000159207	0.001242381
5	0.01	0.003115119	0.001596632	0.01245053
6	0.1	0.03207119	0.01643786	0.12723038

It can be observed the influence of the parameter used for the numerical evaluation of singular integrals on the numerical solution's accuracy. As we can see Mu, Mv, Mcp, vary a lot in relation to eps and their values are smaller as eps get smaller values.

As we notice, looking at the magnitude of the maximum errors, as eps decreases the precision of the numerical solution improves a lot, fact that proves that this parameter has a great impact on the numerical solution and the fact that the procedure used for the numerical evaluation of the singular integrals is a very efficient one.

4.1.2 *The influence of nodes number on numerical solution's accuracy (MQ case)*

The influence of nodes number on numerical solution's accuracy can be studied by letting only this parameter to vary and considering fixed values for the others.

First, we consider different number of nodes and same value for eps and α: $eps = 0.01$, $\alpha = 1$. The absolute errors for the components of velocity and for the local pressure coefficient are presented in the following diagrams, Figure 2.

One can noticed that the errors are similar. For better understanding this influence a comparison by the aid of Mu, Mv and Mcp is made. When $\alpha = 1$, $eps = 0.01$, the diagrams in Figure 3 are obtained.

As we can notice from the above diagrams, the number of nodes does not influence the accuracy of the numerical solution as in case of using BEM to solve the same SBIE [5–7, 9].

As the number of nodes, N, increases, the maximum absolute error, for each of the quantities analyzed, oscillates around a certain value, but the amplitude of this oscillation decreases, and for a large number of nodes, the corresponding limit value is established around this well-defined value, see Figure 3.

The sequence of the maximum errors seems to be convergent to that certain value. Thus, even if in this case, there are no significant differences between the maximum value of the absolute errors obtained for $N = 20$ nodes and the maximum value obtained for $N = 150$ nodes, as N is bigger the numerical procedure is more stable. However, after a certain limit, the accuracy of the numerical solution does no longer improve, as such the computational effort, which is obviously greater, is not justified. Very good numerical results are obtained even for a small number of nodes.

The results were obtained, as mentioned before, in case of $eps = 0.01$ and $\alpha = 1$, and we want to further see if they depend on the considered fixed values, or if similar results are found in other situations too.

The numerical results obtained in case of $eps = 0.001$ and $\alpha = 1$, presented in Figure 4, prove that the dependence is similar in this case too, but in case of a smaller value of eps, the central value toward the maximum errors tend are obvious smaller than in the previous case, as expected, if we think about what was stated previously regarding the influence of eps.

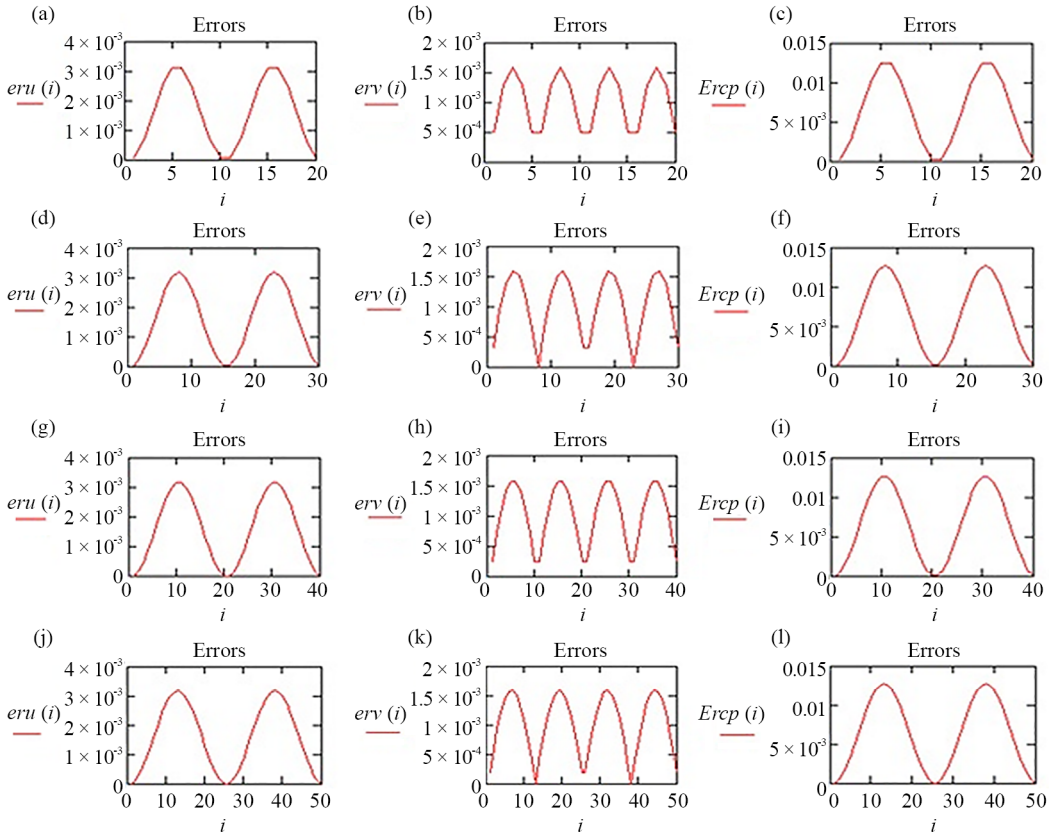

Figure 2. Absolute errors magnitude and distribution for different number of nodes for MQ RBFs, in case of fixed values for the other parameters, namely $eps = 0.01$, $\alpha = 1$

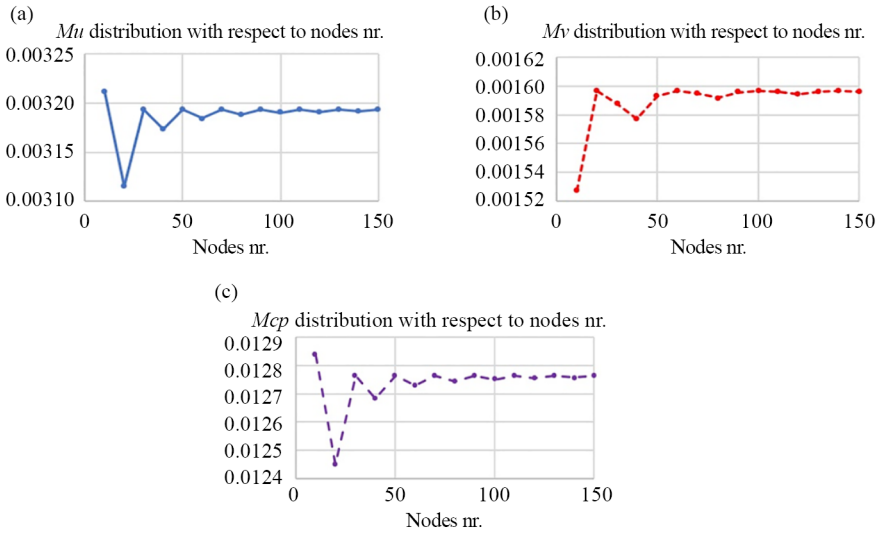

Figure 3. Maximum errors with respect to nodes nr. for MQ RBFs, in case of fixed values for the other parameters, namely $\alpha = 1$ and $eps = 0.010$: (a) *Mu*; (b) *Mv*; (c) *Mcp*

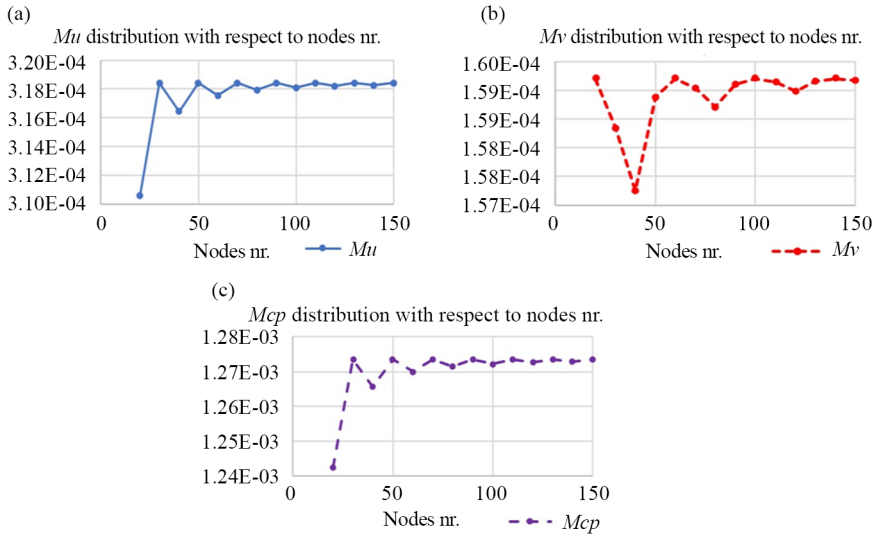

Figure 4. Maximum errors with respect to number of nodes for MQ RBFs, in case of fixed values for the other parameters, namely $\alpha = 1$, $eps = 0.001$: (a) Mu; (b) Mv; (c) Mcp

As we can notice, in Figure 5, same influence of nodes number on the maximum errors exists in case of $eps = 0.0001$ too.

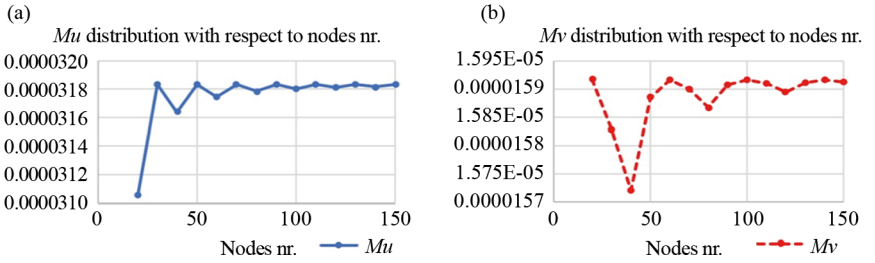

Figure 5. Maximum errors with respect to nr. of nodes for MQ RBFs, in case of fixed values for the other parameters, namely for $\alpha = 1$, $eps = 10^{-4}$: (a) Mu, (b) Mv

4.1.3 *The influence of shape parameter on numerical solution's accuracy (MQ case)*

One of the most important influence on numerical solution's accuracy, when using meshless methods based on RBFs, is of the RBFs shape parameter, α.

In case of using MQ RBFs, errors distribution with respect to α is studied in case of $N = 30$, $eps = 0.001$, for getting the range in which the control parameter must be situated for obtaining numerical solutions of great accuracy. The numerical results are presented in Table 2 and in Figure 6. Simulations were done for 50 values for $\alpha \in [0.000001;\ 2,500]$.

We can observe that if $\alpha \geq 1$ the numerical solution is very good and no major changes arise when α increases to the upper limit 2,500, even beyond this value. The same conclusion can be deduced from Figure 6.

Table 2. Maximum errors with respect to α. ($N = 30$, $eps = 0.001$)

No.	α	Mu	Mv	Mcp
1	0.000001	0.003189633	0.001586379	0.01274836
2	0.00001	0.00318893	0.00158603	0.01274555
3	0.0001	0.00318194	0.001582599	0.01271763
4	0.001	0.003113738	0.001548639	0.01244526
5	0.01	0.002539718	0.001262822	0.01015242
6	0.1	0.000559199	0.000278068	0.002236483
7	1	0.000318411	0.000158334	0.001273544
8	3	0.000318411	0.000158334	0.001273544
9	5	0.000318411	0.000158334	0.001273544
10	10	0.000318411	0.000158334	0.001273544
11	20	0.000318411	0.000158333	0.001273544
12	40	0.000318411	0.000158334	0.001273544
13	50	0.000318411	0.000158334	0.001273544
43	1,800	0.000318411	0.000158336	0.001273545
44	1,900	0.000318411	0.000158337	0.001273544
45	2,000	0.000318412	0.000158337	0.001273546
46	2,100	0.000318412	0.000158335	0.001273545
47	2,200	0.000318411	0.000158336	0.001273543
48	2,300	0.000318412	0.000158338	0.001273546
49	2,400	0.000318411	0.000158337	0.001273544
50	2,500	0.000318411	0.000158337	0.001273544

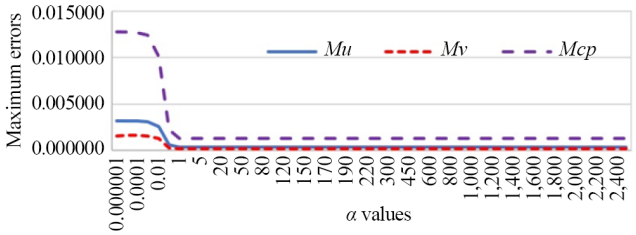

Figure 6. Maximum errors with respect to α for MQ RBFs, in case of fixed values for the other parameters, namely for $N = 30$ and $eps = 0.001$

It may be surprising that the shape parameter can have a wide range of values, in the case when these MQ RBFs appear, to obtain good accuracy. However, to better understand why this happens, we must analyze the context in which these functions appear. We observe that MQ RBF acts as a regularization factor for the singular integrals that appear. Thus, large values of α smooth the integral and therefore we obtain this regularization of the integrals. In case of small α however, we eliminate this regularization, and the singularity becomes more pronounced in the integrand, which leads to a more difficult numerical integration, extremely sensitive, especially for different geometries.

4.2 *Numerical results in case of GA*

Now we consider the case when GA are used for obtaining the numerical solution for the case when an exact one exists, so for the case of an incompressible fluid flow ($M = 0$) and, as in case of MQ RBFs, we study, through an analytical checking, how good the numerical solution is and the influence of the same mentioned parameters (eps, number of nodes, shape parameter) on numerical solution's accuracy.

We choose $N = 20$, $eps = 0.01$, $\alpha = 1$ and we compare, in Figure 7, the numerical results with the exact ones and the distribution of absolute errors, $\overline{eru}$, $\overline{erv}$, $\overline{Ercp}$.

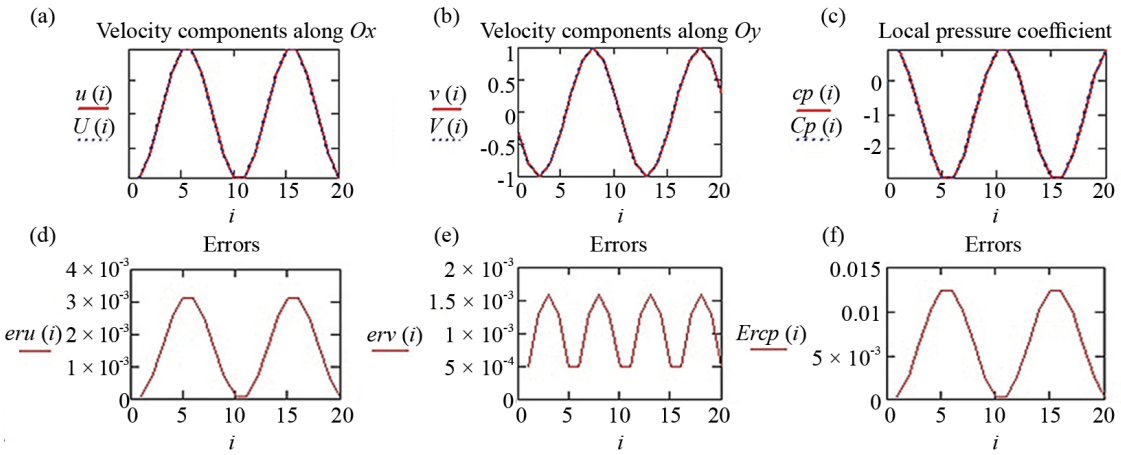

Figure 7. Numerical solution vs. exact one in case of GA RBFs, for $N = 20$, $eps = 0.01$ and $\alpha = 1$

The numerical results are very good in this case too, even for only 20 nodes on the boundary.

4.2.1 *The influence of eps on numerical solution's accuracy (GA case)*

The influence of eps on numerical solution accuracy is study by keeping the same number of nodes, $N = 30$, and $\alpha = 1$ for the control parameter, and varying only eps. The numerical results are presented in Table 3. Same considerations as in case of MQ RBFs can be made: the errors are smaller as eps gets smaller values, and they decrease a lot.

Table 3. Maximum errors with respect to *eps*: $N = 30$, $\alpha = 1$

No.	*eps*	*Mu*	*Mv*	*Mcp*
1	0.000001	3.18329E-07	1.58329E-07	1.27332E-06
2	0.00001	3.18312E-06	1.58286E-06	1.27325E-05
3	0.0001	3.1832E-05	1.58288E-05	0.000127327
4	0.001	0.000318411	0.000158334	0.001273544
5	0.01	0.003193263	0.001587885	0.01276286
6	0.1	0.03287571	0.01634781	0.13042203

4.2.2 *The influence of nodes number on numerical solution's accuracy (GA case)*

For studying the nodes number influence on numerical solution accuracy, we consider different fixed values for *eps* and α and we analyze only *Mu* and *Mv*, without considering *Mcp*, taking into account that the local pressure coefficient is evaluated with the aid of the components of the velocity.

In Figure 8 we remark that we have same pattern as in case of MQ RBFs. When the number of nodes increase the maximum errors tend to a well-defined limit, which value is smaller as *eps* is smaller, and after a certain number of nodes the numerical solution's accuracy does not improve too much, so the numerical effort in such cases is not justified.

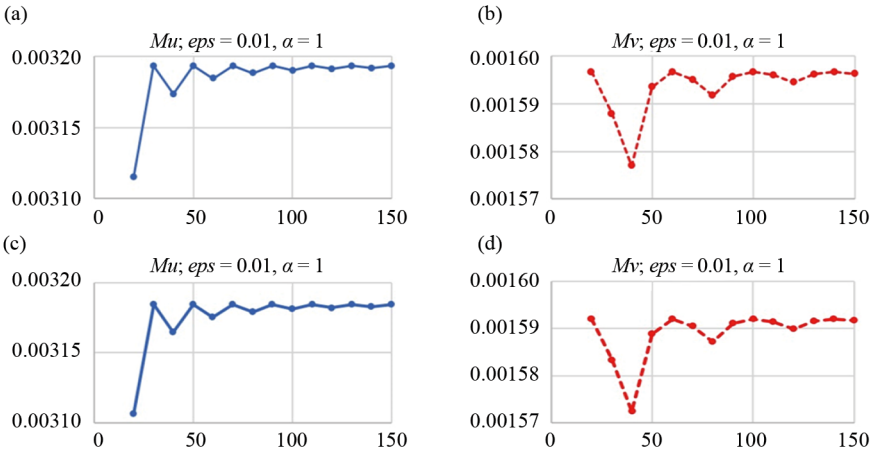

Figure 8. Nodes number influence on numerical solution's accuracy for GA, in case of different values of *eps*: (a) *Mu* in case of $eps = 0.01$, $\alpha = 1$; (b) *Mv* in case of $eps = 0.01$, $\alpha = 1$; (c) *Mu* in case of $eps = 0.001$, $\alpha = 1$; (d) *Mv* in case of $eps = 0.001$, $\alpha = 1$

4.2.3 *The influence of shape parameter on numerical solution's accuracy (GA case)*

The last influence we study is GA shape parameter's influence on numerical solution accuracy. By using computer simulations, taking the advantage of having a case with an exact solution, so the possibility to make an analytical checking, we can deduce an optimal range for the shape parameter.

We consider fixed values for *eps* and *N*, namely $eps = 0.01$, $N = 30$ in the first situation, and $eps = 0.001$, $N = 30$ in the second case. The maximum errors obtained are presented in Table 4, where we have highlighted the optimum range of the GA shape parameter: [0.0005, 5].

Table 4. Maximum errors in relation to α, in case of $N = 30$ and $eps = 0.01$, or $eps = 0.001$

No.	α	$Mu(eps = 0.01)$	$Mv(eps = 0.01)$	$Mu(eps = 0.001)$	$Mv(eps = 0.001)$
1	0.0001	1	0.9945219	1	0.9945219
2	0.0005	0.003193263	0.001587885	0.000318411	0.000158334
3	0.001	0.003193263	0.001587885	0.000318411	0.000158334
4	0.005	0.003193263	0.001587885	0.000318411	0.000158333
5	0.01	0.003193263	0.001587885	0.000318411	0.000158333
6	0.05	0.003193263	0.001587885	0.000318411	0.000158333
7	0.1	0.003193263	0.001587885	0.000318411	0.000158334
8	0.3	0.003193263	0.001587885	0.000318411	0.000158334
9	0.5	0.003193263	0.001587885	0.000318411	0.000158333
10	0.7	0.003193263	0.001587885	0.000318411	0.000158333
11	1	0.003193263	0.001587885	0.000318411	0.000158334
12	2	0.003193263	0.001587885	0.000318411	0.000158341
13	3	0.003193265	0.001587886	0.000318412	0.000158333
14	4	0.003199869	0.00159117	0.000325491	0.000161855
15	5	0.003679054	0.00182945	0.000833027	0.000414232
16	10	0.20068269	0.09979167	0.20173511	0.10031499
17	15	0.46511063	0.23128135	0.4666183	0.23203106
18	20	0.60119218	0.29894939	0.60231832	0.29950938
19	25	0.68175459	0.33900993	0.68264588	0.33945314
20	30	0.73514691	0.36555985	0.73588129	0.36592503
21	40	0.80180913	0.39851777	0.802563	0.40311746

The optimum range can be observed in Figure 9 too, and is the same interval either for $eps = 0.01$, or $eps = 0.001$, so shape parameter's influence is independent of eps values.

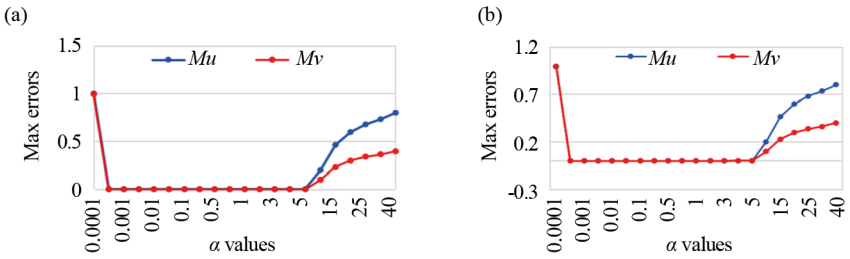

Figure 9. Maximum errors in relation with the shape parameter, α, for GA, in case of different values of eps: (a) Mu, Mv for $eps = 0.01$, $N = 30$; (b) Mu, Mv for $eps = 0.001$, $N = 30$

Shape parameter's influence pattern is the same in both situations, so does not depend on eps value, only the values of the maximum errors are smaller when eps is smaller.

As we can see, small values of α are convenient, as long as they are not too small, because as α approaches 0, the GA function becomes more flat, and goes to a constant, 1. In case of the CPV of integrands with GA kernels, the numerical integration process lead to a less significant contribution of the CPV. It reduces to 0 if α goes to 0. On the other hand, in case of too great values of α, the GA becomes narrow and peaked, having a more pronounced local influence, and in such situations the approximation model does not capture so well the complexity of the unknown variation, especially for a fixed number of nodes, even if it effectively regularizes the singular kernel.

4.3 *Comparisons between different numerical results*

Comparison between MQ RBFs and GA RBFs is made in Figure 10, by considering a value for the shape parameter situated in both optimum ranges, namely we choose $\alpha = 1$, $eps = 0.001$ and 30 nodes on the boundary.

As we can see the numerical solutions are similar, so they do not depend on the type of RBFs considered when applying a meshless method to solve the considered SBIE.

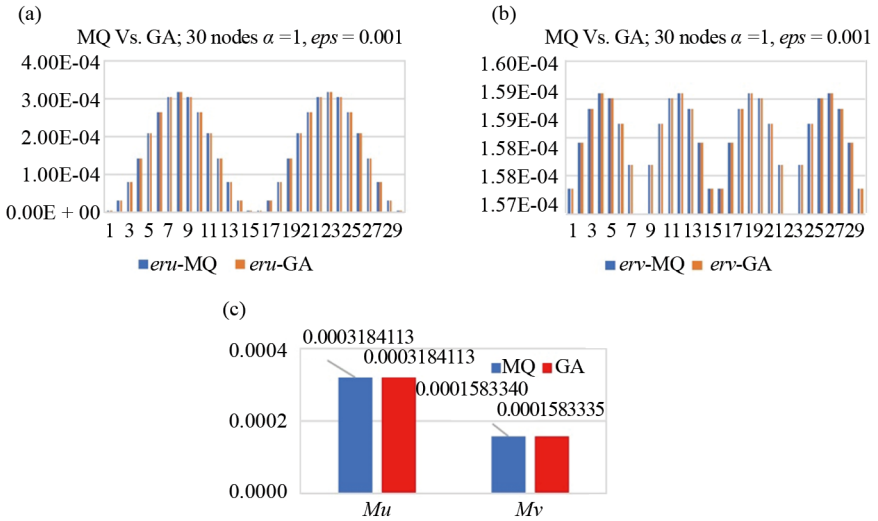

Figure 10. Comparisons between numerical solutions obtained in case of $\alpha = 1$, $eps = 0.001$ and $N = 30$: (a) eru; (b) erv; (c) Mu, Mv

In order to show that the accuracy of the numerical solution is greater when using the present approach to solve the problem of the compressible fluid flow around obstacles then those based exclusively on BEM we have compared the numerical solution with the ones obtained in [6, 7]. The comparison is made in Figure 11 for the components of the velocity field, through the distributions of errors between the numerical solutions and the exact ones for the two components of the velocity field and in Figure 12 through the maximum errors that appear for both components. Because the numerical solutions obtained through this approach do not differ too much for the two types of RBFs we have used, only the numerical solution obtained with GA is considered.

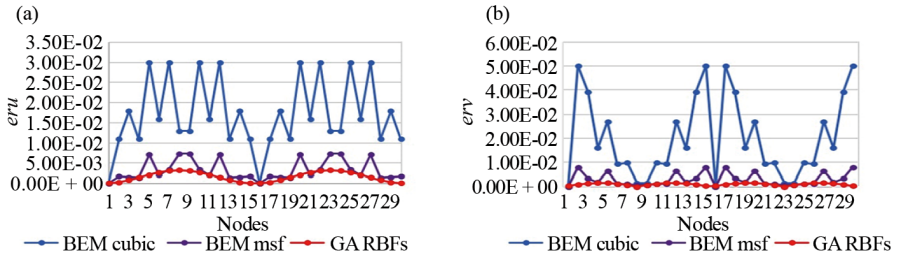

Figure 11. Errors distributions for velocity components for different approaches (BEM cubic, BEM msf, GA RBFs), in case of $eps = 0.01$, $N = 30$, and $\alpha = 1$ when GA are used: (a) *eru*-for velocity component along *Ox*, (b) *erv*-for velocity component along *Oy*

In Figure 11, BEM cubic-represents errors distribution for the numerical solution obtained in [7], where cubic isoparametric boundary elements were used to solve the problem for the same SBIE, and the truncation method to evaluate the integrals of singular kernels. There were considered 30 nodes on the boundary and $eps = 0.01$; BEM msf-represents errors distribution for the numerical solution obtained in [8], where cubic isoparametric boundary elements were also used to solve the same SBIE, but a regu-larization technique with modified shape functions was used to evaluate the integrals of singular kernels; GA RBFs-represents errors distribution for the numerical solution obtained based on the present approach for GA, 30 nodes and $eps = 0.01$.

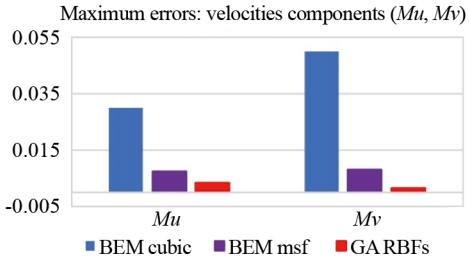

Figure 12. Maximum errors, *Mu* and *Mv*, for the three different numerical solutions (BEM cubic, BEM msf, GA RBFs), in case of $eps = 0.01$, $N = 30$, and $\alpha = 1$ when GA are used

The numerical results are superior in the case of the method proposed in this paper mainly due to the fact that the obstacle boundary is no longer approximated in this case, and the approximation of the unknown is a global one.

The superiority of the present approach also lies in the fact that the numerical codes based on the compared methods using BEM are much more difficult to develop. The approximations of the unknowns being local in these situations, they require the imposition of compatibility conditions when assembling the equations, use more notation systems, more memory and implicitly longer running time. They also cannot be easily adapted for other boundary elements, because both the coefficients of the system and the quantities of interest are very different.

5. Conclusions

The numerical procedure for solving the problem of the compressible fluid flow around obstacles based on an hybrid approach, which consists in starting with a SBIE, an equivalent mathematical model for the mentioned problem, obtained by applying the first step of the BEM, and then solving this SBIE through a meshless method with RBFs is proved to be a very efficient one. Because the problem has, in a particular case, an exact solution, the numerical solutions obtained can be compared with the exact ones and so we can deduce how good the numerical results are and, more than that, we can study the influence of the parameters involved in the procedure, and we refer here at: number of nodes, *eps*-the parameter used for the numerical integration of singular kernels, types of RBFs and α their shape parameter, on the numerical solution's accuracy.

A great advantage of this approach over the classical BEM arises from the fact that when using meshless methods with RBFs we have a global model for the unknown approximation and we only need to choose nodes scattered on the boundary for the unknown interpolation. We don't need to impose connection conditions at nodes, as in case of applying BEM or other discretization techniques, and so the computer code can be easily implemented.

The computer codes developed using Mathcad programming language can be easily adapted for any type of RBFs, not only for MQ or GA. This can be done by only changing the expressions of the RBFs in all evaluated coefficients, because there is no discretization of the boundary, the unknown has a global approximation and the procedure used for the evaluation of the singular kernel integrals does not depend on the type of RBFs, but only on the fact that they are CPVs.

As the graphics show, the numerical and the exact values of the nodal components of the perturbation velocity, of the local pressure coefficient, are in good agreement, even when choosing a small number of nodes on the boundary for both situations. In the present approach the nodes are uniformly distributed on the boundary, which is considered to be closed and smooth, and they also represent the centers of the radial basis function. The uniform distribution is sufficient for obtaining good numerical results because in case of such obstacles we do not need to concentrate nodes near certain special points on the boundary.

The numerical solutions' accuracy obviously depends on the number of nodes chosen on the boundary, but in a different way compared to the procedures that use domain discretization, where the greater the number of nodes, the better the numerical solution is. Here the maximum error oscillates if small numbers of nodes are used on the boundary, and even if the errors are quite similar in case of different number of nodes, the procedure is more stable when using more nodes on the boundary. This number of nodes does not need to be too high in order to obtain a good numerical solution because, as we have seen in this paper, if the number of nodes is too high, exceeding a certain value, the accuracy of the numerical solution no longer increases and the computational effort is not justified.

The procedure used for the singular kernel integrals evaluation (truncation method) is in concordance with the CPV definition of an integral and offers very good results in both cases. The parameter used for the numerical computation of the singular integrals influences a lot the numerical results. The smaller its value is, the better numerical results are obtained.

The numerical solutions' accuracy depends on the shape parameter's value. In both cases when considering values around 1 for this parameter, good numerical solutions are obtained.

The shape parameter's ranges for the two types of RBFs are highlighted, in order to obtain good numerical results: $\alpha \in [1;\ 2,500]$, even for values above the upper limit, in case of MQ, $\alpha \in [0.0005;\ 5]$ in case of GA. These intervals can be used in other approaches to validate theoretical results.

Different types of radial basis functions exist and two of them were used in this approach in order to find out which of them is more suitable for solving the mentioned problem. As proved in the herein paper, the numerical solutions' accuracy does not depend on the type of RBFs, if suitable values for the shape parameters are used, because the maximum errors that appear in the two analyzed cases are quite the same. But, because the optimal range for the shape parameter is larger in case of MQ RBFs, they can be considered the best choice when solving SBIEs through applying meshless methods.

The numerical solutions obtained by the proposed method have a high accuracy, and this is demonstrated in the paper by comparing the numerical solutions not only with numerical ones obtained by other methods, but with exact solutions

that exist in certain special cases. This last comparison allowed the study of the influence of the parameters that appear in the modeling, on the accuracy of the numerical solution.

The proposed hybrid method is a very efficient one because no discretization of the boundary is needed, like in other approaches as those based on FEM, BEM and other procedures based on discretization. For this reason, it is implemented into a very efficient computer code, easy to adapt for any kind of RBFs and for any type of smooth obstacle for which a parametric representation is known. If a parametric representation is not known, a model for the approximation of the boundary has to be used.

The approach proves so, through an analytical checking, that combining the global approximation based on RBFs, with the truncation method for the numerical evaluation of Cauchy-type singular integrals leads to very good numerical results.

The limitations of the method are based on the fact that for other kind of SBIEs there is no guaranty that the range for the optimal values of the shape parameter is the same, but these results can be used for validating further theoretical results regarding finding optimal shape parameters when using RBFs for solving PDEs.

Further work can be focused on developing adaptive strategies to be used to determine the optimal values of the shape parameter in situations when test problems does not exist. It is interesting to study if, for different obstacles of complex geometry, for other subsonic flow regimes (for different Mach number values), or for other type of integral equations, the optimal values of the shape parameter remain in the same range.

Funding

This research did not receive any specific grant from funding agencies in the public, commercial, or not-for-profit sectors.

Conflict of interest

The author declares that she has no competing interests.

References

[1] Pironneau O. *Finite Element Methods for Fluids*. New York: Wiley-Blackwell; 1989.

[2] Howell RH, Spong ED. Numerical solution of subsonic compressible flow at two-dimensional inlets. *AIAA Journal*. 1969; 7(7): 1392-1394.

[3] Wrobel LC. *The Boundary Element Method. Vol. 1: Applications in Thermo-Fluids and Acoustics*. Hoboken, NJ: Wiley; 2002.

[4] Dragoş L. *Mathematical Methods in Aerodynamics*. New York: Springer; 2003.

[5] Grecu L. A solution of the boundary integral equation of the 2D fluid flow around bodies with quadratic isoparametric boundary elements. *ROMAI Journal*. 2006; 2(2): 81-87.

[6] Grecu L. A solution with cubic boundary elements for the compressible fluid flow around obstacles. *Boundary Value Problems*. 2013; 2013: 78. Available from: https://doi.org/10.1186/1687-2770-2013-78.

[7] Grecu L. An improved numerical solution of the singular boundary integral equation of the compressible fluid flow around obstacles using modified shape functions. *Boundary Value Problems*. 2015; 2015: 35. Available from: https://doi.org/10.1186/s13661-015-0294-8.

[8] Brebbia CA, Telles JCF, Wrobel LC. *Boundary Element Theory and Application in Engineering*. Berlin & Heidelberg: Springer-Verlag; 1984.

[9] Grecu L. Radial basis functions for solving the singular boundary integral equation of the compressible fluid flow around obstacles. In: *Proceedings of the International Conference on Applied Mathematics and Numerical Methods (ICAMNM 2020)*. Les Ulis, France: EDP Sciences; 2020. p.2003.

[10] Kansa EJ. Multiquadrics-A scattered data approximation scheme with applications to computational fluid-dynamics-I surface approximations and partial derivative estimates. *Computers & Mathematics with Applications*. 1990; 19(8). Available from: https://doi.org/10.1016/0898-1221(90)90270-T.

[11] Fasshauer GE. Newton iteration with multiquadrics for the solution of nonlinear PDEs. *Computers & Mathematics with Applications*. 2002; 43(3-5): 423-438. Available from: https://doi.org/10.1016/S0898-1221(01)00296-6.

[12] Franke C, Schaback R. Solving partial differential equations by collocation using radial basis functions. *Applied Mathematics and Computation*. 1998; 93(1): 73-82. Available from: https://doi.org/10.1016/S0096-3003(97)10104-7.

[13] Galperin EA, Kansa EJ. Applications of global optimization and radial basis functions to numerical solutions of weakly singular Volterra integral equations. *Computers & Mathematics with Applications*. 2002; 43(3-5): 491-499. Available from: https://doi.org/10.1016/S0898-1221(01)00300-5.

[14] Kansa EJ. Multiquadrics-A scattered data approximation scheme with applications to computational fluid-dynamics-II solutions to parabolic, hyperbolic and elliptic partial differential equations. *Computers & Mathematics with Applications*. 1990; 19(8-9): 147-161. Available from: https://doi.org/10.1016/0898-1221(90)90271-K.

[15] Rana KB, Mavrič B, Zahoor R, Šarler B. A meshless solution of the compressible viscous flow in axisymmetric tubes with varying cross-sections. *Engineering Analysis with Boundary Elements*. 2022; 143: 340-352. Available from: https://doi.org/10.1016/j.enganabound.2022.06.029.

[16] Niraula P, Han Y, Wang J. Comparison of meshfree and mesh-based methods for boundary value problems in physics. *Journal of Physics: Conference Series*. 2015; 640: 12067. Available from: https://doi.org/10.1088/1742-6596/640/1/012067.

[17] Hardy RL. Theory and applications of the multiquadric-biharmonic method 20 years of discovery 1968-1988. *Computers & Mathematics with Applications*. 1990; 19(8-9): 163-208. Available from: https://doi.org/10.1016/0898-1221(90)90272-L.

[18] Buhmann MD. *Radial Basis Functions: Theory and Implementations*. Cambridge, UK: Cambridge University Press; 2003.

[19] Rippa S. An algorithm for selecting a good value for the parameter *c* in radial basis function interpolation. *Advances in Computational Mathematics*. 1999; 11: 193-210. Available from: https://doi.org/10.1023/A:1018975909870.

[20] Hardy RL. Multiquadric equations of topography and other irregular surfaces. *Journal of Geophysical Research*. 1971; 76(8): 1905-1915. Available from: https://doi.org/10.1029/JB076i008p01905.

[21] Fasshauer GE, Zhang JG. On choosing "optimal" shape parameters for RBF approximation. *Numerical Algorithms*. 2007; 45: 345-368. Available from: https://doi.org/10.1007/s11075-007-9072-8.

[22] Azarboni HR, Keyanpour M, Yaghouti M. Leave-Two-Out Cross Validation to optimal shape parameter in radial basis functions. *Engineering Analysis with Boundary Elements*. 2019; 100: 204-210. Available from: https://doi.org/10.1016/j.enganabound.2018.06.011.

[23] Kansa EJ, Hon YC. Circumventing the ill-conditioning problem with multiquadric radial basis functions: Applications to elliptic partial differential equations. *Computers & Mathematics with Applications*. 2000; 39(7-8): 123-137. Available from: https://doi.org/10.1016/S0898-1221(00)00071-7.

[24] Zhang H, Chen Y, Nie X. Solving the linear integral equations based on radial basis function interpolation. *Journal of Applied Mathematics*. 2014; 2014(1): 793582. Available from: https://doi.org/10.1155/2014/793582.

[25] Chen W, Hong Y, Lin J. The sample solution approach for determination of the optimal shape parameter in the Multiquadric function of the Kansa method. *Computers & Mathematics with Applications*. 2018; 75(8): 2942-2954. Available from: https://doi.org/10.1016/j.camwa.2018.01.023.

[26] Aourir E, Izem N, Dastjerdi HL. Numerical solutions of a class of linear and nonlinear Volterra integral equations of the third kind using collocation method based on radial basis functions. *Computational and Applied Mathematics*. 2024; 43: 117. Available from: https://doi.org/10.1007/s40314-024-02630-9.

[27] Mojarrad FN, Veiga MH, Hesthaven JS, Öffner P. A new variable shape parameter strategy for RBF approximation using neural networks. *Computers & Mathematics with Applications*. 2023; 143: 151-168. Available from: https://doi.org/10.1016/j.camwa.2023.05.005.

[28] Li Y, Liu D, Yin Z, Chen Y, Meng J. Adaptive selection strategy of shape parameters for LRBF for solving partial differential equations. *Applied Mathematics and Computation*. 2023; 440: 127645. Available from: https://doi.org/10.1016/j.amc.2022.127645.

[29] Yao G, Chen CS, Zheng H. A modified method of approximate particular solutions for solving linear and nonlinear PDEs. *Numerical Methods for Partial Differential Equations*. 2017; 33(6): 1839-1858. Available from: https://doi.org/10.1002/num.22161.

[30] Ma Y, Chen CS, Hon YC. A novel meshless method for solving long-term evolution problem on irregular domain. *Applied Mathematics and Computation*. 2025; 490: 129209. Available from: https://doi.org/10.1016/j.amc.2024.129209.

[31] Hong Y, Lin J, Chen W. A typical backward substitution method for the simulation of Helmholtz problems in arbitrary 2D domains. *Engineering Analysis with Boundary Elements*. 2018; 93: 167-176. Available from: https://doi.org/10.1016/j.enganabound.2018.05.004.

[32] Ang WT, Wang X. A numerical method based on boundary integral equations and radial basis functions for plane anisotropic thermoelastostatic equations with general variable coefficients. *Applied Mathematics and Mechanics (English Edition)*. 2020; 41(4): 551-566. Available from: https://doi.org/10.1007/s10483-020-2592-8.

[33] Lifanov IK. *Singular Integral Equations and Discrete Vortices*. Utrecht, Netherlands: VSP; 1996.

[34] Antia HM. *Numerical Methods for Scientists and Engineers*. Basel & Boston: Birkhäuser; 2002.